Alpha Particle Irradiation of High Aluminum Content AlGan Polarization Doped Field Effect Transistors

ECS Journal of Solid State Science and Technology, 2020 **9** 035008
2162-8777/2020/9(3)/035008/6/$40.00 © 2020 The Electrochemical Society ("ECS"). Published on behalf of ECS by IOP Publishing Limited

Alpha Particle Irradiation of High Aluminum Content AlGan Polarization Doped Field Effect Transistors

Patrick H. Carey IV,[1,z] Fan Ren,[1,*] Jinho Bae,[2] Jihyun Kim,[2,] and Stephen J. Pearton[3,*]**

[1]*Department of Chemical Engineering, University of Florida, Gainesville, Florida 32608, United States of America*
[2]*Department of Chemical and Biological Engineering, Korea University, Seoul 02841, Republic of Korea*
[3]*Department of Material Science and Engineering, University of Florida, Gainesville, Florida 32608, United States of America*

Alpha particle irradiation at 18 MeV was performed on high aluminum content AlGaN Polarization Doped Field Effect Transistors (POLFTs) and characterized by DC and switching measurements. The POLFETs underwent a reduction in DC saturation current of 23% and 33% at fluences of 1×10^{13} cm^{-2} and 3×10^{13} cm^{-2}, respectively. Carrier removal rates in the range of 2520 cm^{-1} and 7100 cm^{-1} were observed, which are similar to previously reported values for GaN HEMTs. The POLFETs under 100 kHz gate lag measurement demonstrated zero degradation while compared to a traditional GaN HEMT device which suffered serious current collapse as a result of formation of a virtual gate from radiation-induced defects.
 [DOI: 10.1149/2162-8777/ab8019]

Manuscript submitted December 12, 2019; revised manuscript received March 7, 2020. Published March 26, 2020.

Wide bandgap semiconductor materials are promising candidates for electronics systems that would maximize spacecraft efficiency and longevity. The strong chemical bonds present in binary and ternary alloys of III-Nitrides make these intrinsically radiation resistant for total dose applications. A measure of this radiation resistance is the mean displacement energy, which for GaN and SiC are approximately 19.8 eV and 21 eV, respectively, significantly higher than that of GaAs, 9.8 eV.[1] NASA's proposed trip to Venus, with a tentative launch date of 2026 as part of the Venera-D program, is expected to employ SiC technologies for power management and sensor and data handling in the on-board probe.[2]

For extraterrestrial applications, radiation hardness is a key asset which can greatly reduce payload mass and allow for more instrumentation to be included, rather than shielding materials. For interplanetary travel, galactic cosmic rays (GCRs) and solar particle events (SPEs) are the primary sources of radiation. GCRs are composed of 87% hydrogen and 12% helium ions, with heavy ions and electrons making up the last percent.[3] SPEs are composed similarly, with more variation in the heavy ion content.[4] GCRs originate from outside our solar system with an unknown source, since they can easily be deflected, and their direction altered by encountering magnetic fields and intergalactic clouds of other ionized species. SPEs originate from the Sun and occur on a regular cycle. Ejections of energetic particles from the Sun reach the Earth within minutes. When that material encounters the relatively dense atmosphere of Earth, the energetic collisions between these particles and the atmosphere leads to the production of light that we can visually observe, the Aurora Borealis and Aurora Australis.

Alpha particle radiation due to its heavier mass presents a larger risk to both electronics and life forms in space than proton irradiation.[5–20] Alpha particle events in GaN High Electron Mobility Transistors (HEMTs) have been studied previously, although not nearly as well as proton irradiation. Danesin et al. reported on 2 MeV alpha irradiation and noted a 70% reduction on drain current at a fluence of 10^{14} cm^{-2}.[21] Fares et al. reported on 18 MeV alpha irradiation and noted a 41% reduction in drain current at a fluence of 10^{13} cm^{-2}.[22] Additionally, gate lag measurements performed at 100 kHz on the irradiated devices were significantly degraded by approximately 50% from DC measurements, indicating formation of a virtual gate which will limit medium and high frequency performance. The relative damage reported in these two results are as expected, since lower energy particles have a shorter stopping range and undergo more collision events within the active area of the device.

There are several benefits to utilizing an AlGaN Polarization-Doped Field Effect Transistors (POLFETs) over a HEMT structure with the same Al contrast. Primarily, the effects from impurity scattering are removed. This scattering mechanism is characteristic of doped barrier layers in a traditional HEMTs. Another key difference is that the continuous grading of the POLFET induces a 3D electron slab (3DES), rather than the 2D electron gas (2DEG) that is present at the abrupt heterojunction of a HEMT.[23–29] Theoretically this presents the advantage of the mobility being dictated by the higher aluminum content portion of the device rather than the lower aluminum content in the HEMT structure with the same effective aluminum concentration. The near surface electron slab also facilitates Ohmic contact formation over its HEMT counterpart.[23,24,30–32]

In this study, we report an investigated for the first time the effects of alpha particle irradiation on high aluminum content AlGaN POLFETs. The effects were characterized by DC measurement and pulsed characteristics. Stopping Range in Motion (SRIM) modeling was used to elucidate on stopping range and damage mechanisms within the device.

Experimental

The POLFETs were prepared by metal organic vapor phase epitaxy on 1 mm thick (0001) c-plane sapphire mis-oriented by 0.2° towards the *m*-plane. Trimethylammonia, ammonia, and trimethylgallium were used as precursors. The 2.3 μm AlN nucleation and buffer layer was first grown, followed by a subsequent layer of 0.25 μm unintentionally doped $Al_{0.7}Ga_{0.3}N$. The linear grade from 0.7 to 0.85 was accomplished over 110 nm to form the channel. A sheet carrier density of 5.4×10^{12} cm^{-2} and a sheet resistance of 5500Ω/□ were extracted by contactless mercury probe measurements. Circular devices with a gate length of 3 μm and a symmetric drain/source to gate distance of 3.5 μm were fabricated. The gate circumference taken at the center of the gate was 660 μm. Planar Ohmic contacts (Zr/Al/Mo/au) were deposited and annealed, producing a contact resistance of 1.1×10^{-3} Ω-cm^{-2}. A typical Schottky metallization of Ni/Au was used as the gate, which was deposited through an opening in the 100 nm SiN_x passivation, Fig. 1.

An Agilent 4156C Semiconductor Parameter Analyzer was used for DC characterization. Gate lag measurements were taken using an Agilent DSO7054B Oscilloscope, Hewlett–Packard E3615A DC Power Supply, and an Agilent B114A Pulse Generator.

*Electrochemical Society Fellow.
**Electrochemical Society Member.
[z]E-mail: careyph@ufl.edu

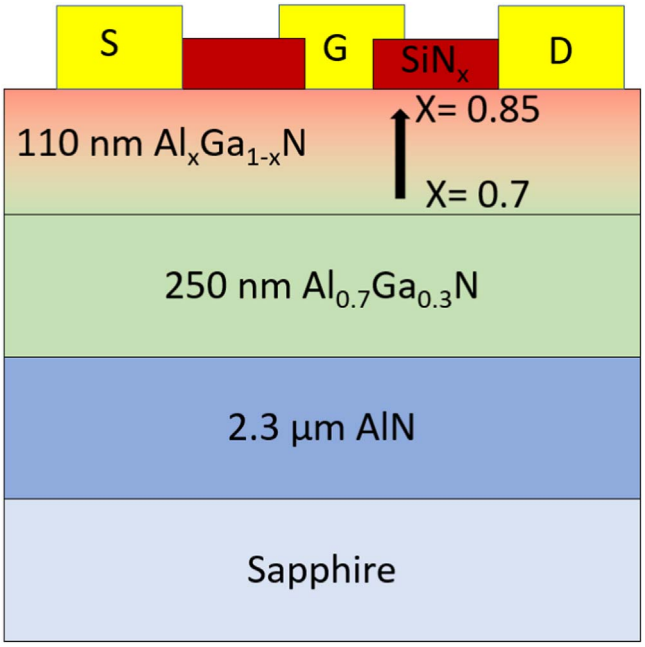

Figure 1. Device schematic of 85/70 POLFET.

Alpha irradiation was perform using a Scanditronix MC 50 cyclotron at the Korean Institute of Radiological and Medical Sciences. The alpha particle energy leaving the cyclotron was 30 MeV, aluminum degraders were used to reduce the energy to 18 MeV before encountering our samples. The flux was monitored via the beam current and a Faraday cup.

Results and Discussion

Before delving into the experimental results, an understanding of the expected damage distribution is necessary. To assist with this, SRIM calculations were done to compare the Coulombic and Nuclear Stopping mechanisms of alpha particles in $Al_{0.7}Ga_{0.3}N$, Fig. 2. The dashed line in these plots denotes the irradiation energy used in this study, 18 MeV. As expected, alpha irradiation (He atoms) undergo significantly greater energy loss in the AlGaN than proton irradiation by both electronic and nuclear stopping, with this trend continuing for higher Z (atomic number) atoms. The stopping power is proportional to Z, due to an increasing interaction cross section and scattering probability. One of the key descriptors of electronic stopping cross section was described by Bethe, considering relativistic effects[33]:

$$-S_e = \frac{4\pi Z_1 e^4}{mv^2} Z_2 \left(\ln\left(\frac{2mv^2}{I}\right) - \ln(1-\beta) - \beta^2 \right) \quad [1]$$

Where S_e is the stopping cross section, Z_1e is the nuclear charge of the incident ion, Z_2e is the nuclear charge of the substrate, m is the mass of an electron, e is the electronic charge of an electron, I is mean excitation energy of the substrate, v is the incident ion speed, and β is v/c with c being speed of light. The shell correction, Barkas correction, and other low energy corrections have been proposed to further to bring (1) in closer alignment with experimental results.[34–37] These will not be considered in this analysis to simplify discussion. From this approximation we can consider that the linear electronic stopping power, S_{lin}, is:

$$S_{lin} = -nS_e = \frac{dE}{dx} \cdot \frac{1}{\rho} \quad [2]$$

where n is the number of target atoms per unit volume, dE/dx is the change in energy over distance traveled through the substrate, and ρ is the density of the substrate. This relation then gives us a direct proportionality between changes in the nuclear charge of the incident ion to the electronic stopping power of the substrate. However, the other key relation is that of the velocity of the incident ion to S_e. Given a fixed kinetic energy of the particle, 18 MeV, hydrogen would be expected to have a 2X greater velocity or 4X greater v^2. These two contributions of a 2X larger nuclear charge of helium and 4 fold lower velocity, give a nearly 1 log difference in electronic stopping power.

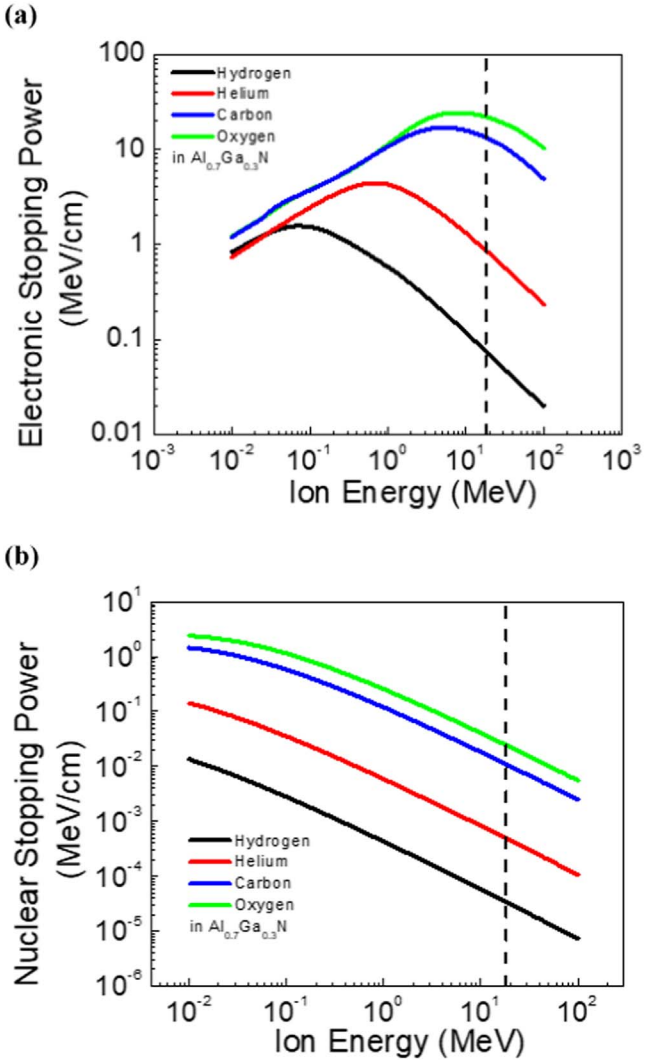

Figure 2. SRIM calculations of (a) electronic stopping power and (b) nuclear stopping power for ions in $Al_{0.7}Ga_{0.3}N$.

Most of the changes in the electrical properties of the semiconductor exposed to alpha particles will be due to displacement damage created by the recoil collisions between the alpha particles and atoms in the solid. The number of collisions of between recoiling target atoms usually far exceeds the number of ion-solid primary recoil collisions. The number of displacements, n_d, is given by the Kitchen–Pease formula,[38]

$$n_d = \frac{E_O}{2E_d} \quad [3]$$

where E_O is the alpha particle energy and E_d is the recoil energy required to displace an atom from its position in the lattice. The factor of 2 arises from an average of all collision paths from those that produce no defects and those that produce only displacements and no energy is lost to electronic stopping or phonon production.

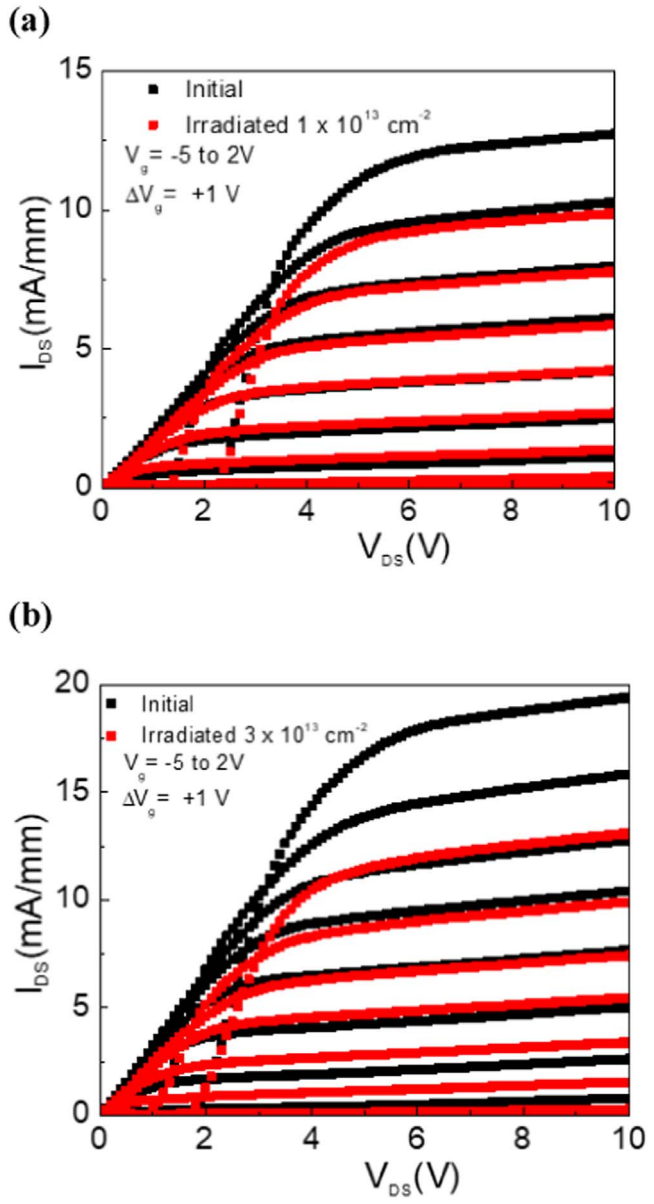

Figure 3. POLFET DC current-voltage characteristics in reference state and irradiated at fluences of (a) 1×10^{13} cm^{-2} and (b) 3×10^{13} cm^{-2}.

More exact calculations involving more realistic atomic potentials and including energy losses for S_e results in the Robinson–Torrens relation[39]

$$n_d = 0.84 \cdot \frac{E_O - Q}{2E_d} \quad [4]$$

where Q is the energy loss associated with S_e.

The next consideration is the type of defects which will be generated by the radiation. The key parameter is the displacement energy of the atoms in the crystal structure. In GaN, ab initio molecular dynamics (AIMD), which agree well with experimental results, found an average displacement energy of 73.2 eV and 32.4 eV for gallium and nitrogen atoms, respectively.[40] In wurtzite AlN, AIMD was again used to determine the minimum displacement energy of 55 eV and 19 eV for aluminum and gallium, respectively.[41] There is a significant dependence on the direction for the displacement energies, but overall, nitrogen is more easily displaced than either Group III element and is the dominant vacancy type expected to be formed under irradiation.

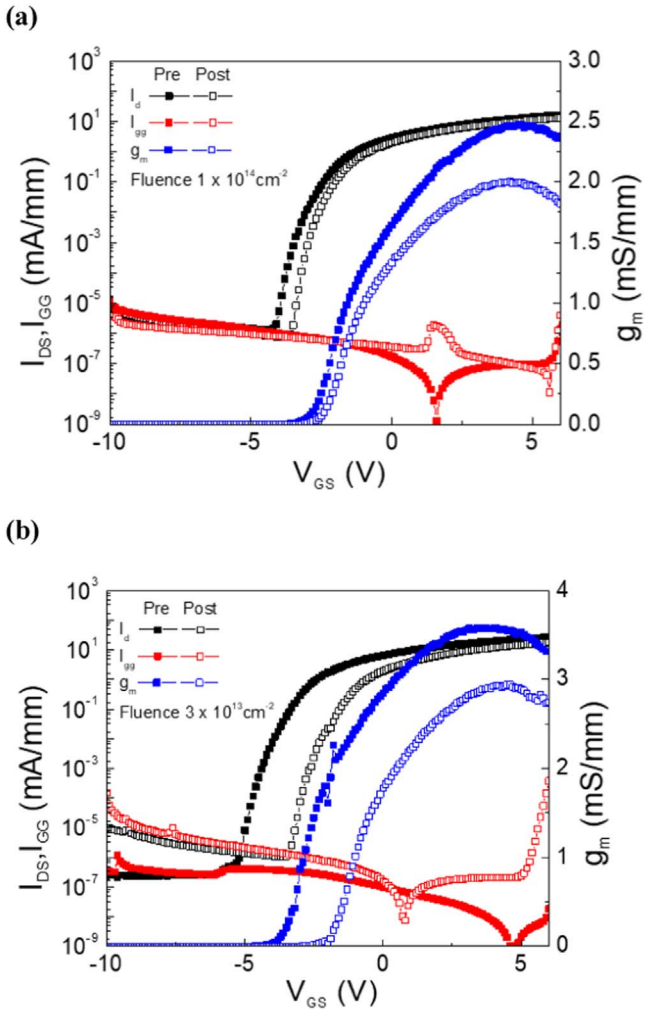

Figure 4. POLFET transfer characteristics in reference state and irradiated at fluences of (a) 1×10^{13} cm^{-2} and (b) 3×10^{13} cm^{-2}.

In Fig. 3, current voltage characteristics are presented for the POLFETs under low dose (1×10^{13} cm^{-2}) and high dose (3×10^{13} cm^{-2}), with forward current reduction of 23% and 33%. The primary DC degradation results from the removal of electron carriers and generation of positively charged traps. Beneath the knee voltage, the slope of the DC output has been reduced, which is indicative of a reduction in electron mobility and carrier concentration.

The transfer characteristics are presented in Fig. 4 and show a large positive shift in the threshold voltage, further indicating a reduction in carrier concentration and the presence of positively charged defects, likely Nitrogen vacancies. The transconductance, g_m, was reduced by 19% and 18% at fluences of 1×10^{13} cm^{-2} and 3×10^{13} cm^{-2}, respectively. No significant change was noted in the subthreshold swing values for either fluence. The gate and drain leakage current only exhibited a slight change at the highest fluence, indicating minimal generation of conducting type defects. The carrier concentration can be related to the shift in threshold voltage by the following relation[42]:

$$n_s = \frac{2\varepsilon qD}{\varepsilon + 2q^2Dd}(V_{gs} - V_{th}) \quad [5]$$

where ε is the dielectric constant of the barrier layer, V_{gs} is the applied gate to source voltage under strong inversion, V_{th} is the threshold voltage, and D is the conduction band density of states where $D = 4\pi m^*/h^2$, m* is the effective electron mass, d is the barrier layer thickness, and h is Planck's constant. From (5) the

values of sheet carrier concentration were calculated and are presented in Table I. The reference state value of $6.54 \times 10^{12}\,cm^{-2}$ is slightly higher than the value extracted by contactless mercury probe CV, $5.4 \times 10^{12}\,cm^{-2}$. This variation could arise from overestimation of the average electron mass within the 3DES, but this difference is small.

The carrier removal rate for low and high dose were 7100 and $2520\,cm^{-1}$, respectively. Ideally the carrier removal rate would be identical for the two doses, as removal rate should only be a function of the energy. This deviation can arise from effects of channeling through the crystalline structure, spatial clustering of defects and saturation of traps that remove carriers at higher doses. The carrier removal rate was plotted against other reported values for lateral HEMT devices, both AlGaN/GaN and InAlN/GaN, Fig. 5. The POLFET structure has a slightly higher reported removal rate in this work than traditional HEMT, this is due to the HEMT containing an atomically thin 2DEG rather than a 55 nm thick 3DES. The alpha particles have a greater vertical distance through the channel to pass and potentially induce defects.

Figure 6 presents the forward gate characteristics for devices exposed to the highest fluence. Nominal change was noted in the gate leakage current when the drain was not biased. The barrier height of the gate was extracted via the thermionic emission model:

$$I = I_0 \exp\left(\frac{qV}{nkT}\right)\left[1 - \exp\left(-\frac{qV}{kt}\right)\right] \quad [6]$$

$$I_0 = AA^{**}T^2 \exp\left(-\frac{q\phi_b}{kT}\right) \quad [7]$$

where I_0 is the reverse saturation current, V is the applied voltage, n is the ideality factor, A is effective diode area, A** is the Richardson constant, k is the Boltzmann constant, and ϕ_b is the barrier height. The extracted Schottky barrier heights and ideality factors are presented in Table II. The barrier height lowering of 0.22 eV and 0.64 eV at fluences of $1 \times 10^{13}\,cm^{-2}$ and $3 \times 10^{13}\,cm^{-2}$, respectively, is consistent with the observed degradation in drain leakage current presented in the transfer characteristics, shown in Fig. 3.

Gate-lag measurements were performed to evaluate the medium frequency power switching of the devices and observe any effects of the formation of a virtual gate. The devices were operated at 100 kHz and 10%–50% duty with a drain bias of +10 V. Figure 7 shows the gate lag for the POFLET and a reference SiN_x/AlGaN/GaN MISHEMT that was irradiated simultaneously. The presence of a virtual gate, leading to a surface depletion region, caused a significant reduction in drain current in the reference MISHEMT sample. Scattering within the channel from irradiation induced defects and virtual gate formation are significant under switching operation. However, the POLFET sample shows essentially no change other than an overall reduction in current from the lower carrier concentration. This performance is unique-while scattering effects still occur, they are primarily confined within the 55 nm 3DES and the electrons do not necessarily leave the electron channel and become trapped in the buffer layer to form a virtual gate.

To confirm the result of the GaN HEMT devices suffering major current collapse under switching operation there are two other

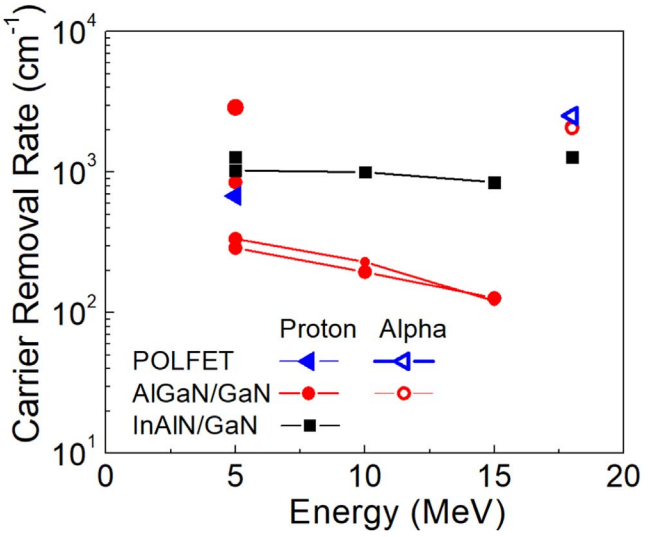

Figure 5. Comparison of carrier removal rates for radiation damaged POLFETs and previously reported GaN HEMT based lateral devices as a function of radiation energy and type.[5–10,22]

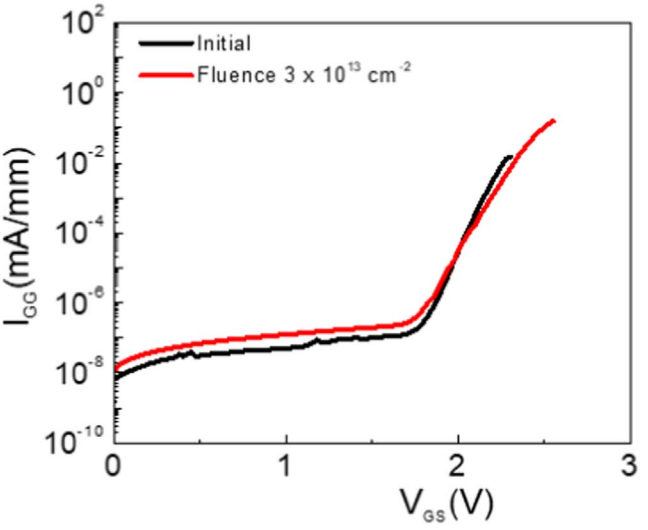

Figure 6. Forward I_{gg}-V_g used for extraction of Schottky barrier height and ideality factor.

comparable works: Danesin et al.[5] and Fares et al.[6] The literature available on the effects of alpha particle irradiation is significantly less than proton irradiation, for which GaN HEMT is well studied. Danesin et al. used a MOCVD grown GaN/AlN/$Al_{0.35}Ga_{0.65}N$ heterostructure. A low-frequency gate-lag measurements at 0.66 Hz and 33% duty showed a loss of 20% of on current for a fluence of $10^{13}\,cm^{-2}$. At such low frequency few conclusions can be drawn about the formation of a virtual gate within this work. The work of Fares et al. used a GaN/AlGaN/SiN_x heterostructure and performed gate-lag characterization at sufficient frequency such that a comparison can be better drawn. Under 100 kHz and 10% duty, at

Table I. Sheet carrier concentrations and carrier removal rates.

Sample	n_s (cm^{-2})	% Carrier Reduction	Carrier Removal Rate (cm^{-1})
Reference $1 \times 10^{13}\,cm^{-2}$	6.55×10^{12}	—	—
Irradiated $1 \times 10^{13}\,cm^{-2}$	5.77×10^{12}	11.9	7100
Reference $3 \times 10^{13}\,cm^{-2}$	6.51×10^{12}	—	—
Irradiated $3 \times 10^{13}\,cm^{-2}$	5.68×10^{12}	12.8	2520

Table II. Schottky barrier height and ideality factor extracted via the thermionic emission model.

Sample	n	SBH (eV)
Reference 1 × 10^{13} cm^{-2}	1.69	1.87
Irradiated 1 × 10^{13} cm^{-2}	2.96	1.65
Reference 3 × 10^{13} cm^{-2}	1.58	1.89
Irradiated 3 × 10^{13} cm^{-2}	3.10	1.25

a fluence of 10^{12} cm^{-2} current collapse was 65% of the DC value. This work with the POLFETs used an order of magnitude higher fluence (1 × 10^{13} cm^{-2} and 3 × 10^{13} cm^{-2}) and only observed nominal difference in the DC value to the pulsed values, regardless of duty cycle.

It is interesting to contrast the results described here for alpha particle irradiation with our previous studies of the effects of proton irradiation on these same device structures.[9] The proton irradiation in that case was performed at fluences of 1 × 10^{14} cm^{-2} and 3 × 10^{14} cm^{-2} at 10 MeV. From Eqs. 1 and 2, a helium ion deposits nearly an order of magnitude more energy into displacement damage at a given energy than a hydrogen ion. As such, using an order of magnitude lower fluence with alpha radiation should produce similar degradation as observed in the proton irradiation when dose is accounted for. While the energy in[9] is not identical to the energy used for alpha particles in this work, the shift in stopping power for 10 MeV vs 18 MeV in Fig. 1 for protons is small. The reduction of DC current in the proton work was 24% and 48% at low and high dose, respectively, these values are slightly higher than that produced by the alpha irradiation at low and high dose (23% and 33%). Reduction in peak transconductance was greater under proton irradiation at 21% and 36% as compared to 19% and 18% for low and high dose, respectively, In both DC current and transconductance the degradation for proton irradiated devices was worse than the alpha particle irradiated devices, this may be partially attributed to the related effects of dehydrogenation of defects[19,43,44] and also the likely more efficient recombination of primary interstitial point defects with lattice vacancies in the case of alpha particles. The final level of damage is a balance of defect creation and recombination rates and is strongly dependent on target temperature and dose rate during irradiation.

While the majority of the incident protons/alpha particles will pass through the active layer, some will be deposited within the active region. An alpha particle upon neutralization will become helium, an inert atom. However, a hydrogen atom will seek to passivate a crystal defect or form H_2. As the incident protons are creating defects as they pass through the semiconductor, the likelihood of forming H_2 is unlikely considering the atomic density of a semiconductor is usually the order of 10^{20} or 10^{21} atoms cm^{-3} and the proton fluence used is 10^{14} cm^{-2}. A hydrogenated defect is not necessarily stable and under on-state conditions hot electrons within the channel can release the hydrogen given the electron's kinetic energy is greater than the activation energy of the hydrogen passivated defect.[43,44] This will form a negatively charged defect upon release, such as $[V_{Ga}H_2]^-$ or $[V_{Al}H_2]^-$, which will reduce forward current and transconductance.[44]

Conclusion

In this work, the effects of alpha irradiation on high aluminum content POLFETs were determined at a beam energy of 18 MeV and fluences of 1 × 10^{13} cm^{-2} and 3 × 10^{13} cm^{-2}. Fluence was observed to have a direct but not directly proportional effect over this fluence range on the reduction in drain current, transconductance, and carrier concentration. The lowering of the barrier height of the Schottky metal gate was observed to have direct effect on an increase in drain leakage current. 100 kHz switching operation was used to identify the presence of electron traps. The POLFET showed

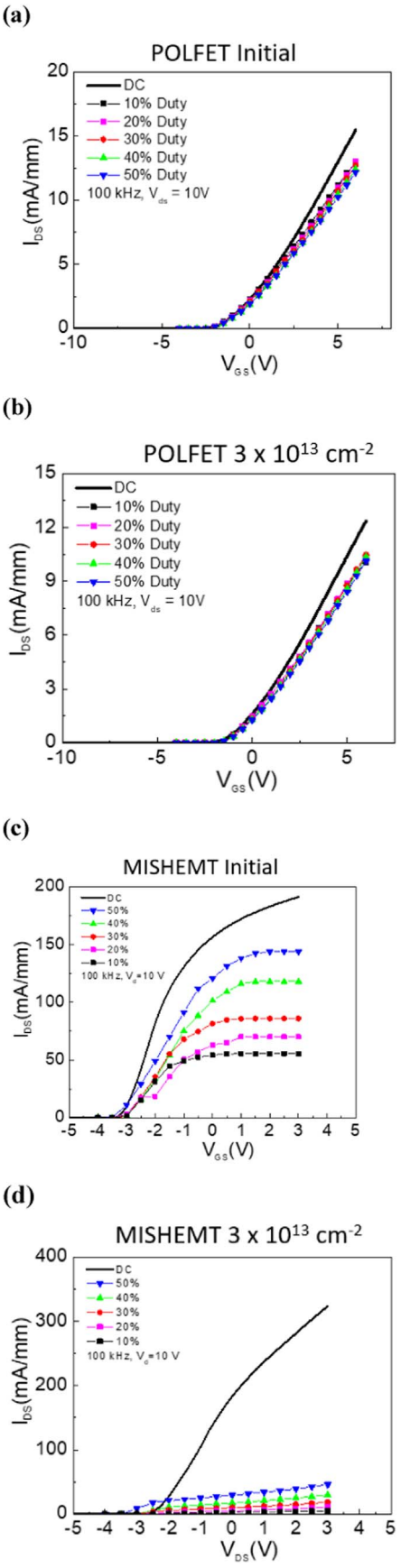

Figure 7. Gate-lag measurements performed at 100 kHz, V_{ds} = 10 V, and duty cycle 10%–50% for POLFETs, (a) initial and (b) fluence of 3 × 10^{13} cm^{-2}, and MISHEMTs, (c) initial and (d) fluence of 3 × 10^{13} cm^{-2}.

no degradation at either fluence while operating at 100 kHz., in sharp contrast to traditional MISHEMTs, which underwent significant current collapse. This work has demonstrated the high potential for this type of device in highly radiative environments over traditional GaN and may extend device lifetime significantly.

Acknowledgments

The work at UF was partially sponsored by the Department of the Defense, Defense Threat Reduction Agency, No. HDTRA1-17-1-011, monitored by Jacob Calkins. The research at Korea University was supported by the National Research Foundation of Korea (2018R1D1A1A09083917) and the Korea Institute of Energy Technology Evaluation and Planning (KETEP) (20172010104830).

ORCID

Patrick H. Carey IV https://orcid.org/0000-0002-8826-3977
Jihyun Kim https://orcid.org/0000-0002-5634-8394
Stephen J. Pearton https://orcid.org/0000-0001-6498-1256

References

1. A. Ionascut-Nedelcescu, C. Carlone, A. Houdayer, H. J. von Bardeleben, J. L. Cantin, and S. Raymond, "Radiation hardness of gallium nitride." *IEEE Trans. Nucl. Sci.*, **49**, 2733 (2002).
2. *Phase II Report Venera-D: Expanding Our Horizion of Terrestrial Planet Climate and Geology Through the Comprehensive Exploration of Venus* (2019), https://lpi.usra.edu/vexag/reports/Venera-DPhaseIIFinalReport.pdf.
3. G. D. Badhwar and P. M. O'Neill, "Galactic cosmic radiation model and its applications." *Adv. Space Res.*, **17**, 7 (1996).
4. T. L. Garrard and E. C. Stone, "Composition of energetic particles from solar flares." *Adv. Space Res.*, **14**, 589 (1994).
5. L. Liu, C. Cuervo, Y. Xi, F. Ren, S. J. Pearton, H.-Y. Kim, J. Kim, and I. Kravchenko, "Impact of proton irradiation on dc performance of AlGaN/GaN high electron mobility transistors." *Journal of Vacuum Science & Technology B, Nanotechnology and Microelectronics: Materials, Processing, Measurement, and Phenomena*, **31**, 042202 (2013).
6. L. Liu et al., "Dependence on proton energy of degradation of AlGaN/GaN high electron mobility transistors." *Journal of Vacuum Science & Technology B, Nanotechnology and Microelectronics: Materials, Processing, Measurement, and Phenomena*, **31**, 022201 (2013).
7. S. Ahn, B.-J. Kim, Y.-H. Lin, F. Ren, S. J. Pearton, G. Yang, J. Kim, and I. Kravchenko, "Effect of proton irradiation dose on InAlN/GaN metal-oxide semiconductor high electron mobility transistors with Al_2O_3 gate oxide." *Journal of Vacuum Science & Technology B, Nanotechnology and Microelectronics: Materials, Processing, Measurement, and Phenomena*, **34**, 051202 (2016).
8. S. Ahn, C. Dong, W. Zhu, B.-J. Kim, Y.-H. Hwang, F. Ren, S. J. Pearton, G. Yang, J. Kim, and I. Kravchenko, "Study on effect of proton irradiation energy in AlGaN/GaN metal-oxide semiconductor high electron mobility transistors." *ECS Trans.*, **69**, 129 (2015).
9. P. H. Carey, F. Ren, J. Bae, J. Kim, and S. J. Pearton, "Proton irradiation of high aluminum content AlGaN polarization doped field effect transistors." *ECS J. Solid State Sci. Technol.*, **9**, 025003 (2020).
10. Y. Xi et al., "Effect of 5 MeV proton radiation on DC performance and reliability of circular-shaped AlGaN/GaN high electron mobility transistors." *Journal of Vacuum Science & Technology B, Nanotechnology and Microelectronics: Materials, Processing, Measurement, and Phenomena*, **32**, 012201 (2014).
11. B. Weaver, T. J. Anderson, A. D. Koehler, J. D. Greenlee, J. K. Hite, D. I. Shahin, F. J. Kub, and K. D. Hobart, "Editors' choice—on the radiation tolerance of AlGaN/GaN HEMTs." *ECS J. Solid State Sci. Technol.*, **5**, Q208 (2016).
12. A. D. Koehler et al., "Proton radiation-induced void formation in Ni/Au-Gated AlGaN/GaN HEMTs." *IEEE Electron Device Lett.*, **35**, 1194 (2014).
13. J. D. Greenlee, P. Specht, T. J. Anderson, A. D. Koehler, B. D. Weaver, M. Luysberg, O. D. Dubon, F. J. Kub, T. R. Weatherford, and K. D. Hobart, "Degradation mechanisms of 2 MeV proton irradiated AlGaN/GaN HEMTs." *Appl. Phys. Lett.*, **107**, 083504 (2015).
14. J. C. Gallagher, T. J. Anderson, A. D. Koehler, N. A. Mahadik, A. Nath, B. D. Weaver, K. D. Hobart, and F. J. Kubb, "Effect of surface passivation and substrate on proton irradiated AlGaN/GaN HEMT transport properties." *ECS J. Solid State Sci. Technol.*, **6**, S3060 (2017).
15. T. J. Anderson, D. J. Meyer, A. D. Koehler, J. A. Roussos, B. D. Weaver, K. D. Hobart, and F. J. Kub, "Impact of 2 MeV proton irradiation on the large-signal performance of Ka-band GaN HEMTs." *ECS J. Solid State Sci. Technol.*, **6**, S3110 (2017).
16. T. J. Anderson, A. D. Koehler, J. A. Freitas Jr., B. D. Weaver, J. D. Greenlee, M. J. Tadjer, E. A. Imhoff, K. D. Hobart, and F. J. Kub, "Hyperspectral electroluminescence characterization of OFF-state device characteristics in proton irradiated high voltage AlGaN/GaN HEMTs." *ECS J. Solid State Sci. Technol.*, **5**, Q289 (2016).
17. S. J. Pearton, F. Ren, E. Patrick, M. E. Law, and A. Y. Polyakov, "Review—ionizing radiation damage effects on GaN devices." *ECS J. Solid State Sci. Technol.*, **5**, Q35 (2015).
18. C. Fares, F. Ren, S. J. Pearton, G. Yang, J. Kim., C.-F. Lo, and J. W. Johnson, "Effect of proton irradiation energy on SiNx/AlGaN/GaN metal-insulator semiconductor high electron mobility transistors." *Journal of Vacuum Science & Technology B*, **36**, 052202 (2018).
19. J. Chen et al., "Proton-induced dehydrogenation of defects in AlGaN/GaN HEMTs." *IEEE Trans. Nucl. Sci.*, **60**, 4080 (2013).
20. J. Chen et al., "Effects of applied bias and high field stress on the radiation response of GaN/AlGaN HEMTs." *IEEE Trans. Nucl. Sci.*, **62**, 2423 (2015).
21. F. Danesin, F. Zanon, S. Gerardin, F. Rampazzo, G. Meneghesso, E. Zanoni, and A. Paccagnella, "Degradation induced by 2-MeV alpha particles on AlGaN/GaN high electron mobility transistors." *Microelectron. Reliab.*, **46**, 1750 (2006).
22. C. Fares, F. Ren, S. J. Pearton, G. Yang, J. Kim., C.-F. Lo, and J. W. Johnson, "Effect of alpha-particle irradiation dose on SiNx/AlGaN/GaN metal–insulator semiconductor high electron mobility transistors." *Journal of Vacuum Science & Technology B*, **36**, 041203 (2018).
23. A. M. Armstrong, B. A. Klein, A. G. Baca, A. A. Allerman, E. A. Douglas, A. Colon, V. M. Abate, and T. R. Fortune, "AlGaN polarization-doped field effect transistor with compositionally graded channel from $Al_{0.6}Ga_{0.4}N$ to AlN." *Appl. Phys. Lett.*, **114**, 052103 (2019).
24. A. M. Armstrong, B. A. Klein, A. Colon, A. A. Allerman, E. A. Doublas, A. G. Baca, T. R. Fortune, V. M. Abate, S. Bajaj, and S. Rajan, "Ultra-wide band gap AlGaN polarization-doped field effect transistor." *Jpn. J. Appl. Phys.*, **57**, 074103 (2018).
25. D. Jena, S. Heikman, D. F. Green, I. B. Yaacov, R. Coffie, H. Xing, S. Keller, S. Denbaars, J. S. Speck, and U. K. Mishra, "Realization of wide electron slabs by polarization bulk doping in graded III–V nitride semiconductor alloys." *Appl. Phys. Lett.*, **81**, 4395 (2002).
26. G. Li, R. Wang, B. Song, J. Verma, Y. Cao, S. Ganguly, A. Verma, J. Guo, H. G. Xing, and D. Jena, "Polarization-induced GaN-on-Insulator E/D Mode p-Channel Heterostructure FETs." *IEEE Electron Device Lett.*, **34**, 852 (2013).
27. M. Qi, K. Namoto, M. Zhu, Z. Hu, Y. Zhao, B. Song, G. Li, P. Fay, H. Xing, and D. Jena, "High-voltage polarization-induced vertical heterostructure p-n junction diodes on bulk GaN substrates." *2015 73rd Annual Device Research Conference*, p. 31 (2015).
28. S. Rajan, H. Xing, S. DenBaars, U. K. Mishra, and D. Jena, "AlGaN/GaN polarization-doped field-effect transistor for microwave power applications." *Appl. Phys. Lett.*, **84**, 1591 (2004).
29. J. Simon, V. Protasenko, C. Lian, H. Xing, and D. Jena, "Polarization-induced hole doping in wide-band-gap uniaxial semiconductor heterostructures." *Science*, **327**, 60 (2010).
30. B. A. Klein et al., "Planar ohmic contacts to $Al_{0.45}Ga_{0.55}N/Al_{0.3}Ga_{0.7}N$ high electron mobility transistors." *ECS J. Solid State Sci. Technol.*, **6**, S3067 (2017).
31. S. Bajaj, F. Akyol, S. Krishnamoorthy, Y. Zhang, and S. Rajan, "AlGaN channel field effect transistors with graded heterostructure ohmic contacts." *Appl. Phys. Lett.*, **109**, 133508 (2016).
32. E. A. Douglas, S. Reza, C. Sanchez, D. Koleske, A. Allerman, B. Klein, A. M. Armstrong, R. J. Kaplar, and A. G. Baca, "Ohmic contacts to Al-rich AlGaN heterostructures." *physica status solidi (a)*, **214**, 1600842 (2017).
33. H. Bethe, "Bremsformel fr Elektronen relativistischer Geschwindigkeit." *Zeitschrift fr Physik*, **76**, 293 (1932).
34. U. Fano, "Penetration of protons, alpha particles, and mesons." *Annual Review of Nuclear Science*, **13**, 1 (1963).
35. P. T. Leung, "Addendum: 'Bethe stopping-power theory for heavy-target atoms'." *Phys. Rev. A*, **60**, 2562 (1999).
36. W. H. Barkas, J. N. Dyer, and H. H. Heckman, "Resolution of the Σ−-mass anomaly." *Phys. Rev. Lett.*, **11**, 26 (1963).
37. J. Lindhard, "The Barkas effect - or Z13, Z14-corrections to stopping of swift charged particles." *Nucl. Instrum. Methods*, **132**, 1 (1976).
38. G. H. Kinchen and R. S. Pease, "The displacement of atoms in solids by radiation." *Reports of Progress in Physics*, **18**, 1 (1955).
39. M. T. Robinson, "The influence of the scattering law on the radiation damage displacement cascade." *Philos. Mag.*, **12**, 741 (1965).
40. H. Y. Xiao, F. Gao, X. T. Zu, and W. J. Weber, "Threshold displacement energy in GaN:Ab initiomolecular dynamics study." *J. Appl. Phys.*, **105**, 123527 (2009).
41. J. Xi, B. Liu, Y. Zhang, and W. J. Weber, "Ab initio molecular dynamics simulations of AlN responding to low energy particle radiation." *J. Appl. Phys.*, **123**, 045904 (2018).
42. A. Rashmi, S. Kranti, Haldar, and R. S. Gupta, "An accurate charge control model for spontaneous and piezoelectric polarization dependent two-dimensional electron gas sheet charge density of lattice-mismatched AlGaN/GaN HEMTs." *Solid-State Electronics*, **46**, 621 (2002).
43. Y. S. Puzyrev, T. Roy, B. R. Tuttle, R. D. Schrimpf, D. M. Fleetwood, and S. T. Pantelides, "Dehydrogenation of defects and hot-electron degradation in GaN high-electron-mobility transistors." *J. Appl. Phys.*, **109**, 034501 (2011).
44. J. Ren, D. Yan, W. Mou, Y. Zhai, G. Yang, and X. Gu, "Hot electrons induced degradation in lattice-matched InAlN/GaN high electron mobility transistors." *Microelectron. Reliab.*, **56**, 34 (2016).